Advanced Steel Construction – Vol. 21 No. 1 (2025) 21–30
DOI:10.18057/IJASC.2025.21.1.2

INDUSTRIAL FLOOR CONSTRUCTION JOINT – EXPERIMENTAL AND NUMERICAL ANALYSIS

Isidora Jakovljević [1, *], Nina Gluhović [1], Milan Spremić [1] and Dušan Rajnović [2]

[1] *University of Belgrade, Faculty of Civil Engineering, Belgrade, Republic of Serbia*
[2] *Rinol d.o.o, Belgrade, Republic of Serbia*
** (Corresponding author: E-mail: isidora@imk.grf.bg.ac.rs)*

ABSTRACT

Transverse plane joints of concrete industrial ground floors are mostly constructed with various steel dowel geometry and arrangements to provide effective shear load transfer and prevent differential vertical movements. Several features of the construction joints can lead to the loss of the joint serviceability and resistance requirements, such as geometry misalignment, corrosion and joint lockup upon concrete casting. In addition, subsequent deterioration and damage of the exposed edges of the concrete surfaces have been indicated, influencing the serviceability of industrial floors and maintenance difficulties. Newly introduced construction joint geometry represents a functional solution of free-movement joints towards increasing construction efficiency and prevention of joint geometry misalignment and joint lockup upon concrete casting. The paper presents experimental tests and a comprehensive finite element analysis of the behaviour of the integral construction joint with steel dowels and embedded formwork. The experimental campaign covered testing of two orientations of the newly introduced construction joint to shear load. Numerical finite element analysis including the parametric study was performed to complement experimental results and reach a final stage of joint efficiency.

ARTICLE HISTORY

Received: 30 April 2024
Revised: 20 November 2024
Accepted: 30 November 2024

KEYWORDS

Steel dowel;
Free-movement joint;
Concrete ground floor;
Finite element method;
Shear resistance;
Dowel design analysis

1. Introduction

Transversal construction joints, designed to relieve longitudinal stresses due to volumetric changes in large concrete panels (surfaces), can be generally classified into two groups: construction joints for concrete pavements of highways and airports, and construction joints for concrete industrial ground floors and exterior pavements. Within these two main groups, various geometries of construction joints have been designed and examined, considering the differences in level and frequency of applied load and serviceability requirements or other structural issues that directly affect the safe and efficient use of concrete pavements and floors. Nevertheless, construction joints must fulfil the main requirements: to maintain horizontal movements of the concrete slab panels due to expansion and contraction and to transfer vertical loads between adjoining slabs [1]. The demand for construction joint application in large concrete panels originates also from interrupted construction activities during concrete casting [2].

Dowels are the most common form of construction joints which are used to provide smooth transition between adjoining concrete slab panels and to prevent cracking due to volumetric phenomena such as expansion and shrinkage, but also warping and curling caused by temperature and moisture gradients across the depth of the concrete slab [3]. Steel dowels (steel bars or plate dowels) are the most often used type of construction joints. Epoxy coatings for steel dowels are usually applied to prevent corrosion susceptibility. However, it has been reported that corrosion remains still a potential issue that affects the resistance and serviceability requirements [4] since the epoxy coating is susceptible to damage during the concrete casting and service life of the pavement [3]. Despite the reduction of dowel surface due to corrosion and its direct influence on joint resistance, corrosion also results in joint lockup. Construction joint lockup leads to the prevention of lateral movement of concrete slab and flexibility of construction joint, therefore mislaying the main function and consequently resulting in spalling, joint faulting and mid-span cracking [4].

Joint lockup and distress of the construction joint can also be influenced by misalignment of the joint geometry upon the concrete casting [4]. Misalignments of the steel dowel can be classified into two main groups: translation which represents movement of the constriction joint in horizontal, vertical or longitudinal direction and therefore offset from the concrete central plane and rotational misalignment of the joint which is the result of the joint tilting [1]. Zuzulova et al. [5] reported in their investigation that vertical tilt (rotational misalignment) of dowel bars results in high concrete tensile stresses around the dowel. Laboratory tests pointed to the higher tensile stresses for traditionally used 25 mm diameter dowels in comparison to the 30 and 40 mm dowels diameter and therefore suggest the increase of dowels diameter to 30 mm in highways. Experimental tests and finite element analysis of the steel and Glass Fibre Reinforced Polymer (GFRP) dowel bars' performance when they are installed with different geometry misalignments are in detail presented in the work of Al-Humeidawi and Mandal [1], [4]. Also, the aforementioned investigation highlights the influence of non-uniform misalignment of the dowels over the transverse joint length on the joint lockup and therefore achieved pull-out load for the joint opening during the tests. The same investigation also resulted in comparable characteristics of 38 mm GFRP dowel diameter with 25 mm epoxy-coated steel dower bar considering dowel looseness and relative deflection of the construction joint. Also, a substantial reduction in pull-out load for the joint opening during the investigation was achieved using GFRP dowel bars [4].

The GFRP and stainless steel dowel bars can be a suitable alternative to the mostly used epoxy-coated steel dowel bars considering corrosion susceptibility and were in detail investigated in the previous period. Dowels in construction joints often fail due to excessive bearing stress in the concrete surrounding the dowel resulting the cracks in concrete [6], since it is the principal mechanism in load transfer. Fasil et al. [3] found out that GFRP dowel bars fail due to the shear in the transverse direction considering the low shear capacity and high tensile strength of the embedded glass fibers. According to Vijay et al. [7] the stiffness mismatch between steel dowel and concrete localises the load transfer region at a higher level and results in concrete cracking near the steel dowel in comparison to the application of dowels with lower material stiffness. GFRP dowel bars have a lower elastic modulus in comparison to the steel ones and therefore should be applied with 20–30% larger diameter or in smaller distances across the transversal joint length to achieve comparable behaviour considering resistance, deflections and concrete bearing stresses in case of heavy loads [3]. However, for most of the concrete industrial ground floors, the application of GFRP dowel bars with smaller diameters is achievable for low frequency of heavy loads. Despite the higher costs of the GFRP dowels (approximately 50%), the long-term maintenance costs are less in comparison to the steel dowels [2].

According to ACI 302.1R-04 [8], concrete ground slabs continue to shrink for years, while the most significant volumetric change takes place within the first 60 to 90 days and continues through the first year till the fourth year upon concrete casting. Opening of the joint is a result of fulfilled service requirements of the construction joint but also can affect the serviceability requirements and safe and efficient use of the concrete pavements and floors. Maintenance of the construction joints represents a specific aspect of the overall inspection and maintenance of the concrete surfaces (floors). Available design guides for construction joints, ACI 302.1R-04 [8] and Technical Report 34 [9], propose an application of different types of joint sealants or low viscosity fillers, during the lifetime of the applied construction joint to balance between the ability to achieve joint opening, but also to prevent deterioration and damage of the exposed edges of the concrete surfaces.

However, 3D finite element analyses of steel and GFRP dowel bars give a wider insight into the behaviour of the construction joints and have been reported in many works [10], [11], [12], [13], [14]. Together with experimental tests or real environment monitoring of construction joints, numerical 3D analyses of the previous period resulted in findings which were implemented in

technical reports and design procedures. Certain directions for the design of construction joints including recommended dowel size and spacing, depending on the concrete slab depth, are provided in the American Concrete Institute Guide for Concrete Floor and Slab Construction ACI 302.1R-04 [8]. Technical Report 34 [9] published by The Concrete Society, UK, prescribes analytical expressions for obtaining design resistance of joints with round and plate dowels, and defines the classification of joints according to the movement they allow and the method by which they are formed. Therefore, construction joints are classified as free-movement joints, restrained-movement joints, tied joints and isolation joints. Free-movement joints, which are the main focus of the forthcoming investigation through experimental and numerical investigation, should be applied between the floor ground slab and adjoining such as external pavements and dock leveller or machine base. This type of joint has the potential to open wider than restrained-movement joints, without the application of reinforcement across the joint and therefore dowels or other mechanisms should provide load transfer. Construction joints should be designed to reduce vertical movement to the minimum.

Here presented previous works are mostly focused on the behaviour of various dowels as construction joint components. Limited laboratory testing on the resistance and response of the overall construction joints with embedded formworks as integral solutions for industrial floors is indicated. In the current study, experimental testing and 3D finite element analysis of the free-movement construction joint for concrete industrial ground floors are presented. The study took into account the aforementioned features of the construction joints which lead to loss of the joint serviceability and resistance requirements. Therefore, a new type of free-movement construction joint was investigated, through several aspects of higher construction accuracy of the joint geometry, lower misalignments of steel dowels and highly reduced potential in joint lockup considering well-integrated design and construction process. Towards more functional joint geometry, a numerical parametric study was performed to complement experimental results and reach a final stage of joint efficiency.

2. Experimental programme

2.1. Construction joint geometry

The geometry of the newly introduced construction joint is given in Fig. 1. Several parts of the free-movement construction joint were designed and assigned individually or simultaneously with other parts to improve the geometry during construction interruptions, prevent joint lockup, reduce vertical deformations and enable efficient load transfer. The presented construction joint, which is a subject of further experimental and numerical analysis, can be installed in industrial floors as an integral structural solution.

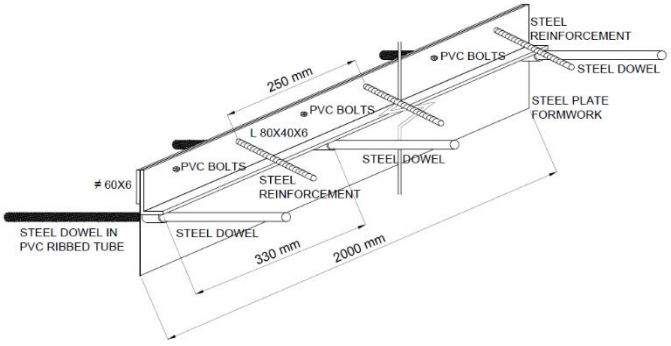

Fig. 1 Construction joint geometry

Three main constructive parts of the analysed construction joint, given in Fig. 1, are (i) steel plate of 60 mm height and 6 mm thickness, (ii) steel hot-rolled angle profile L 80 x 40 x 6 mm, and (iii) steel dowel of 22 mm diameter and overall length through construction joint of 500 mm. Among those three main constructive parts, additional parts of the construction joint are (a) PVC ribbed tube, (b) steel plate formwork of 1–2 mm thickness, (c) 10 mm diameter steel reinforcement bars welded to the 60 mm steel plate and angle profile, (d) steel tube leader of 26 mm outside diameter and 4 mm thickness, and (e) PVC bolts. Steel dowels are positioned on 330 mm spacing over the length of the construction joint, while reinforcement bars are welded at a 250 mm distance (Fig. 1). Steel dowels are placed in the middle of the height of the construction joint.

Described construction joint parts carrying a specific function should provide following: a) steel plate of dimensions of 60 x 6 mm together with steel plate of 1–2 mm thickness represent integral formwork for interrupted construction activities during concrete casting; b) steel angle profile enables sufficient stiffness of formwork to maintain initial geometry of the joint during concrete casting and therefore providing main free-movement characteristics of the joint; c) PVC ribbed tube wraps the steel dowel at the half length of the construction joint achieving in certain amount additional anti-corrosion protection, providing free movement of the steel dowel inside construction joint and preventing the joint lockup; d) PVC bolts supply the joint with integral geometry, preventing the separation of the steel plate and angle profile during installation and concrete casting, but also high longitudinal flexibility for undemanding opening of the construction joint due to volumetric changes, e) steel tube leader positioned on the side of the angle profile provides bearing surface to the steel dowels in order to minimize vertical and horizontal misalignments of the steel dowels; f) steel reinforcement prevents deterioration and damage of the exposed edges of the concrete surfaces and provides additional anchoring of steel formwork and angle profile in concrete slab on both sides.

2.2. Test set-up and loading protocol

The geometry of the specimens with the new construction joint is given in Fig. 2. Two orientations of the construction joint within test series R1 and R2 were investigated through experimental tests and 3D finite element analysis. Three specimens were tested for both test series, six specimens overall.

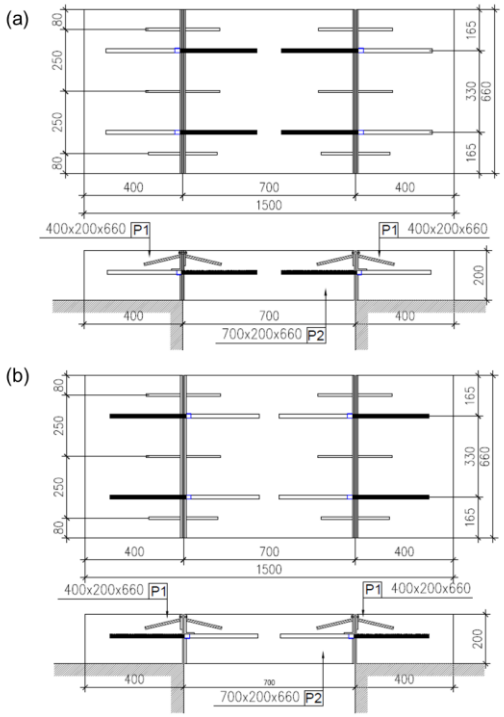

Fig. 2 Geometry of the specimens: (a) R1 series, (b) R2 series

Specimens were designed and constructed as double shear specimens with two side slabs and one middle (loaded) slab which were connected with construction joints. The overall dimensions of the specimens were 1500 x 660 mm, with 400 mm width of side slabs, 700 mm width of the middle slab and 200 mm depth of each slab. Construction joint within tests series R1 was installed with angle profile and steel dowel placed in the side slabs, i.e. steel dowel with PVC ribbed tube and 60 x 6 mm steel plate were positioned in the middle (loaded) slab (Fig. 2a). The opposite direction was adopted for test series R2, therefore angle profile and steel dowel were positioned in the middle (loaded) slab (Fig. 2b). The overall geometry of the specimens was in detail measured after the installation, showing the maximum misalignment of 3% in the vertical position of steel dowels in comparison to the middle plain of the concrete slab. Two layers of Q355 reinforcement mesh of 8 mm diameter were positioned at the bottom layer of the middle slab to prevent bending slab failure before the resistance of the construction joint is achieved. To analyse the resistance and overall behaviour of the construction joint in the most unfavourable conditions, when the joint has achieved the expected opening in industrial ground floors of approximately 10 mm, the polystyrene foam sheet was installed between 60 x 6 mm steel plate and angle profile.

Double shear tests were performed through the application of the linear vertical load in the middle width of the loaded slab through a stiff hot-rolled steel

profile with adequate flange width, not affecting the failure region of the concrete close to the construction joint, but accomplishing uniform and symmetrical loading of both joints. Stiff supports were provided at the end of the side slabs to prevent horizontal movement of the slabs or their rotation (Fig. 3). Vertical movement at the position of load application was monitored with LVDTs of the hydraulic testing machine, but also with two additional LVDTs, labelled as P1 and P2 in Fig. 3a. Relative vertical movement between two slabs at the position of the construction joints was measured with four LVDTs (V1–V4), symmetrically placed considering the load position and overall geometry of the specimens. Additionally, vertical movement was controlled at the position of the support of the side slabs with two LVDTs (O1 and O2) to monitor the efficiency of the support structure.

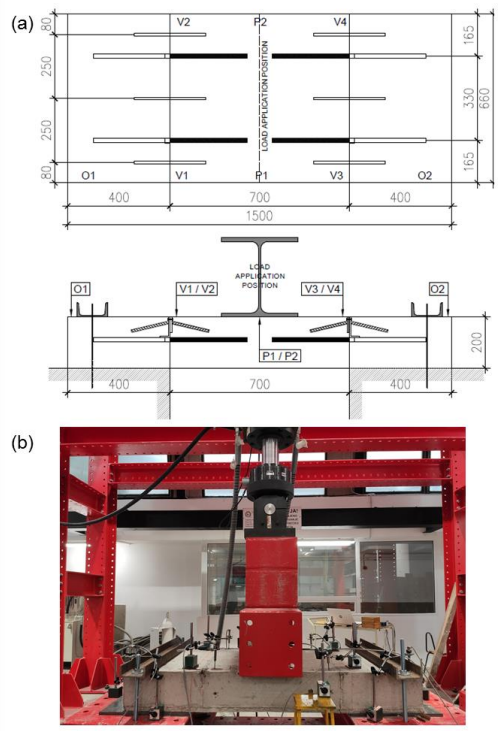

Fig. 3 Test set-up: (a) measuring positions, (b) specimen during testing

A hydraulic testing machine with a capacity of 300 kN was used for specimen testing. Specimens were tested through two phases. Within the first phase, cyclic loading was applied through three cycles with load in the range from 5 kN to 20 kN, with 0.2 kN/s. Upon reaching the 20 kN of vertical load, the loading of the specimen was maintained constant for 40 s and consequently unloaded with the same load rate of 0.2 kN/s until 5 kN. The first phase of the specimen testing was performed within 10 min, followed by the second phase of loading until failure. The load of the second testing phase was introduced as displacement controlled with a loading rate of 0.015 mm/s, therefore failure was not achieved within 15 min of the second loading phase [15]. The testing continued until the load dropped by 20% of the ultimate load.

2.3. Material properties

Alongside the main experimental testing, material properties of concrete and steel components of construction joints were obtained through standardised testing procedures. Concrete compressive strength was determined by conducting tests on concrete cubes 150 x 150 x 150 mm. Prisms 120 x 120 x 360 mm and cylinders Ø150 x 150 mm were used to obtain concrete flexural and splitting tensile strength, respectively. The mean and characteristic values of concrete strength on the day of the testing of specimens' series R1 and R2 are provided in Table 1.

Table 1
Material properties of concrete

	Compressive strength $f_{c,cube}$	Flexural strength $f_{ct,fl}$	Splitting tensile strength $f_{ct,sp}$
Mean value [MPa]	59.4	3.83	4.15
CoV [%]	3.01	1.39	10.23
Characteristic [MPa]	54.7	3.65	2.72

Mechanical properties of steel dowel, angle profile and 60 x 6 mm steel plate, as the main constructive elements of the construction joint, were determined from coupon tensile tests according to the ISO 6892-1 [16]. The values of steel yield and tensile strength, as well as strain at ultimate strength and fracture strain, are summarized in Table 2.

Table 2
Material properties of steel components of the construction joint

Steel component	Yield strength			Ultimate strength			Strain at ultimate strength	Strain at fracture
	Mean f_y [MPa]	CoV [%]	Charact. f_{yk} [MPa]	Mean f_u [MPa]	CoV [%]	Charact. f_{uk} [MPa]	Mean ε_u [%]	Mean ε_f [%]
Steel dowel	333.4	1.36	318.0	458.8	0.02	458.4	20.39	36.79
Angle profile L 80 x 40 x 6 mm	316.1	3.96	273.9	458.4	0.34	453.2	20.28	35.50
Steel plate 60 x 6 mm	343.9	/	/	482.1	/	/	19.08	34.30

Table 3
Evaluation of construction joint resistance and deformation

Specimen	Ultimate load F_{max} [kN]	Vertical displacement		Stiffness $k_{70\%}$ [kN/mm]*
		at 70% of the ultimate load $V_{70\%}$ [mm]	at the ultimate load V_{ULT} [mm]	
R1-1	168.8	2.59	3.58	10.17
R1-2	165.7	2.59	4.81	11.05
R1-3	199.4	2.78	3.19	12.55
Mean value, m_x	177.95	2.65	3.86	11.26
Characteristic fractile factor, k_n	3.37			
St. deviation, s	18.61			
Characteristic value, R_k	115.25			
R2-1	143.1	2.61	3.93	9.58
R2-2	121.1	1.21	2.28	17.52
R2-3	144.2	2.63	3.89	9.59
Mean value, m_x	136.15	2.15	3.37	12.23
Characteristic fractile factor, k_n	3.37			
St. deviation, s	13.07			
Characteristic value, R_k	92.11			

*obtained per one steel dowel at 70% of the ultimate load

2.4. Experimental results

Results of the experimental analysis are given in Fig. 4, for two analysed test series R1 and R2, respectively, as the applied load in function of the vertical displacement at the position of the construction joint measured with LVDTs with designation V1–V4. In addition, the results of the tests are given in Table 3 through the resistance of the construction joint, vertical displacement for load corresponding to 70% of ultimate load, vertical displacement for ultimate load and the stiffness of the construction joint, together with statistical evaluation of the results according to the EN 1990 – Annex D [17].

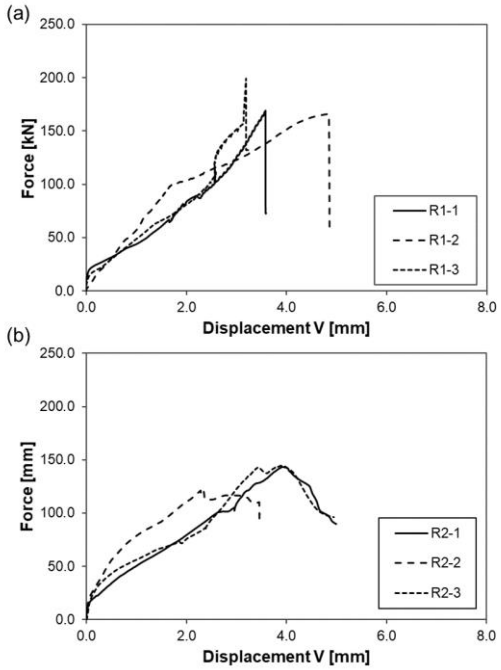

Fig. 4 Experimental test results – force-displacement at joint: (a) R1 series, (b) R2 series

According to the test results gained from two test series, approximately 31% higher resistance was obtained for test series R1 (177.95 kN) than for test series R2 (136.15 kN) when the resistance mean values of the two series are compared. The characteristic resistance of test series R1 determined according to the EN 1990 – Annex D [17] is approximately 25% higher in comparison to the test series R2.

Moreover, the different performance of the construction joint within the two test series is evident when comparing the construction joint post-ultimate response, described through force-displacement curves in Fig. 4. All specimens of test series R1 are characterized by a sudden decrease of the resistance upon the maximum force is reached, while a much slower decrease of the resistance is achieved for test series R2, indicating potentially different failure modes for the two test series.

Evaluation of the obtained deformation of the construction joint is analysed through measurements of the V1–V4 LVDTs, at the position of the construction joint. The mean value of the vertical displacement for the loading level corresponding to 70% of the ultimate load for test series R1 is 3.86 mm, which is to some extent increased in comparison to the 3.37 mm for test series R2. The mean value of the analysed stiffness for test series R1 and R2 are 11.26 kN/mm and 12.23 kN/mm, respectively, indicating relatively uniform behaviour of both test series considering the stiffness per one steel dowel obtained for 70% of the ultimate load. Larger vertical displacement at the ultimate load for test series R1 follows the results obtained for the load corresponding to 70% of the ultimate load. The mean value of vertical displacement for ultimate load is 2.65 mm for test series R1 and 2.15 mm for test series R2. This is approximately 23% higher vertical displacement for test series R1 in comparison to series R2, corresponding to approximately 31% higher resistance.

For all tested specimens within two test series, concrete failure close to the construction joint in the middle (loaded) slab is achieved. Fig. 5 represents the vertical surface of the middle slab when the maximum load is reached. Although diagonal cracks occurred in all tested specimens in both vertical surfaces of the middle slab, they do not represent the governing failure mode of the construction joint, which is in more detail described through numerical analysis.

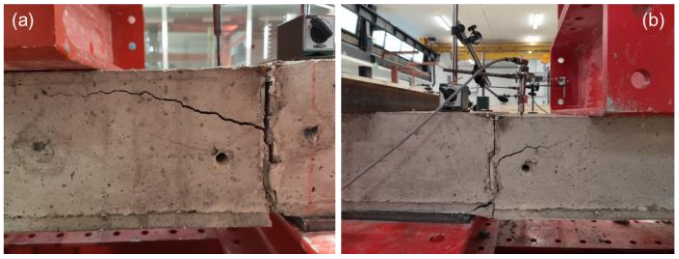

Fig. 5 Cracks on the middle slab – vertical surface of the test specimens: (a) R1 series, (b) R2 series

Upon the testing, construction joints were relatively simply disassembled (Fig. 6), highlighting the high-performance characteristics of the free-movement joint. Significant deformation of the construction joint upon the testing was not observed. Embedded steel formwork remained unaffected, while steel dowels were subjected to certain, but not distinct deformation during the testing procedure, according to Fig. 6.

Fig. 6 Construction joint upon the testing

The presented results demonstrate the straightforward influence of the construction joint orientation on the behaviour of the construction joint with particular emphasis on shear resistance and post-ultimate response. Specimens within test series R1, where the angle profile and steel dowels of the construction joint are placed in side slabs of double-shear tests, obtained higher resistance in comparison to the opposite orientation of the construction joint. Specimens within test series R2, where the angle profile and steel dowels of the construction joint are positioned in the middle (loaded) slab obtained more ductile behaviour in comparison to the test series R1.

3. Finite element numerical analysis

3.1. Development of finite element models

Numerical models were developed to simulate the experimental testing, evaluate specimen behaviour and failure modes, and perform further parametric analysis. 3D models were developed in finite element software Abaqus [18], performing the geometrical and material nonlinear analysis in the Dynamic Explicit solver.

3.1.1. Model geometry

According to the experimental programme, two 3D finite element models were created representing the test series R1 and R2, with the opposite orientations of the construction joint. Numerical models simulated the double shear test conditions, with two side concrete slabs connected to the middle concrete slab through the construction joint. The symmetry of tested specimens was exploited by modelling a quarter of the specimen and applying appropriate double vertical symmetry conditions, as illustrated in Fig. 7a. All relevant components of the construction joint were modelled, including round dowels, steel plate and angle profile, reinforcement bars for plate and angle anchoring, PVC ribbed tubes and steel plate 1–2 mm thickness with steel tube leader. Moreover, the base plate for bearing slabs was created, as well as the bottom reinforcement mesh in the middle slab. The components of the numerical model were solid parts, except for the reinforcement mesh and plate of 1–2 mm thickness, which were modelled as a truss and shell, respectively.

3.1.2. Boundary conditions, interactions and loading

Vertical loading was applied through the reference point RP1 on the middle slab top surface, whereas fully fixed boundary conditions were added to the reference point RP2 on the bottom surface of the base plate, as presented in Fig. 7a. Reference points were constrained to the nodes on the corresponding surface, accounting for the width of the loaded area. Welded connection between

components of the construction joint was simulated using the tie constraint. Reinforcement mesh was connected to the concrete slab by the embedded constraint. Contacts between other parts were simulated through "hard" contact in the normal direction and friction contact in the tangential direction. Values on friction coefficients were assigned as: 0.45 for contacts between concrete and steel or plastic parts embedded in concrete, as well as for the contact between the side slab and the supporting plate, 0.30 for the contact between dowel and plastic sleeve, and 0.20 for the contact between dowel and steel tube.

The vertical loading was applied through the smooth step function as a displacement-controlled. The total duration of the simulation was set to 1000 s with the mass scaling time increment of 0.005 s.

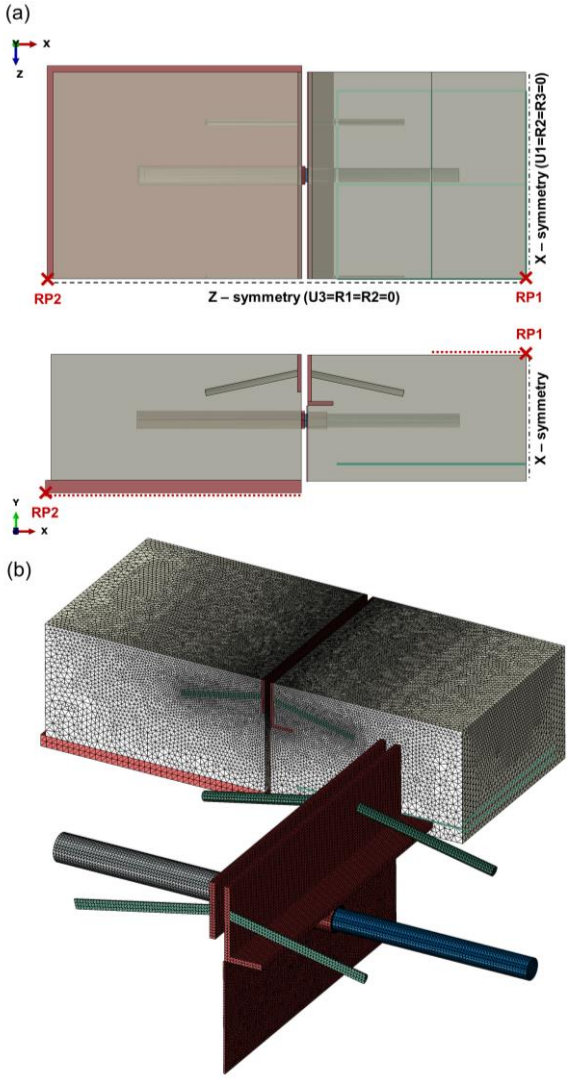

Fig. 7 Model R2: (a) Model geometry and boundary conditions, (b) Finite element mesh

3.1.3. Finite element mesh

Due to the complex geometry of the developed model, tetrahedral finite elements C3D10M were selected for meshing solid parts. Similarly, S3 elements were used for meshing shell parts and T3D2 elements were used for truss parts. The adopted mesh size resulted from the convergence analysis conducted to optimize the computing time while providing accurate model behaviour. Finite element size was varied throughout the model, applying the smallest size elements of 3 mm to steel dowels and other components of the construction joint. The mesh size was then gradually increased throughout the concrete slabs in the range from 3 mm at the construction joint to 10 mm at the opposite slab edges, according to Fig. 7b.

3.1.4. Material models

Material behaviour was assigned to the numerical model according to the performed testing of steel coupons and concrete cubes.

Elastic properties of steel were defined through the modulus of elasticity of 210 GPa and Poisson's ratio of 0.3. The plastic response of the steel dowel, angle profile and steel plate was modelled through the appropriate true stress-strain curves based on the conducted experimental tensile tests. As reinforcement bars were not experimentally tested, their response was modelled according to EN 1992-1 [19] as elastic-perfectly plastic with a yield strength of 500 MPa.

The behaviour of the plastic sleeve was simulated by assigning the modulus of elasticity of 1 GPa, Poisson's ratio of 0.2, and perfect plastic response with a yield strength of 50 MPa.

Concrete behaviour was described using the Concrete Damage Plasticity model. Concrete response in the elastic domain was defined through the modulus of elasticity of 35.11 MPa and Poisson's ratio of 0.2. The plasticity parameters were set following the recommended values in the Abaqus user manual [18]: flow potential eccentricity of 0.1, the ratio of equibiaxial-to-uniaxial compressive strength of 1.16, and a parameter K of 0.67. The dilation angle was set to the value of 30°, according to Lubliner et al. [20].

The stress-strain relation for describing concrete behaviour to uniaxial compression was adopted according to the model proposed by Pavlović et al. [21], which demonstrated good accuracy in simulating the steel-concrete shear connections accomplished with various types of steel connectors [22–26]. For strains up to ε_{cu1} (between points A and D in Fig. 8a), the stress-strain relation is described through the expression provided in EN 1992-1-1 [19]:

$$\sigma_c(\varepsilon_c) = f_{cm}\frac{k\cdot\eta - \eta^2}{1 + (k-2)\eta},\ \varepsilon_c \le \varepsilon_{cu1} \tag{1}$$

where:

$$\eta = \frac{\varepsilon_c}{\varepsilon_{c1}} \tag{2}$$

$$k = 1.05\,\varepsilon_{c1}\frac{E_{cm}}{f_{cm}} \tag{3}$$

ε_{c1} is a compressive strain in the concrete at the maximum stress fcm,
$\varepsilon_{cu1} = \varepsilon_{cuD}$ is the ultimate compressive strain of concrete.

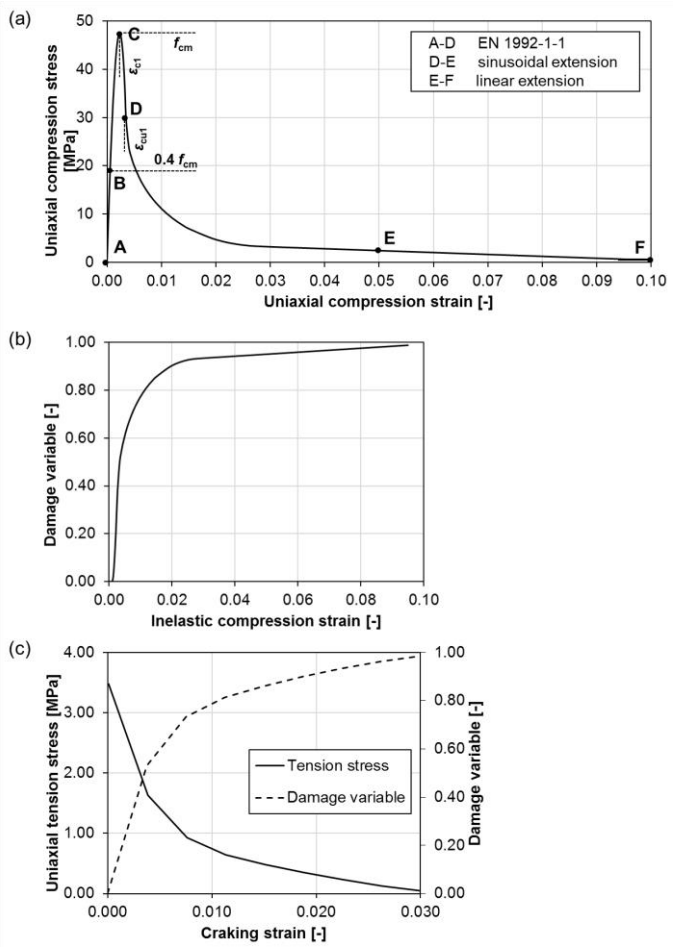

Fig. 8 (a) Concrete stress-strain relation for compression, (b) Concrete damage in compression, (c) Concrete behaviour in tension

For strains beyond ε_{cu1}, the stress-strain curve is based on the sinusoidal (for strains smaller than ε_{cuE}, between points D and E in Fig. 8a) and linear extension (for strains larger than ε_{cuE}, between points E and F in Fig. 8a):

$$\sigma_c(\varepsilon_c) = \begin{cases} f_{cm}\left[\frac{1}{\beta} - \frac{\sin(\mu^{\alpha_{tD}}\cdot\alpha_{tE}\,\pi/2)}{\beta\cdot\sin(\alpha_{tE}\,\pi/2)} + \frac{\mu}{\alpha}\right], \varepsilon_{cuD} < \varepsilon_c \le \varepsilon_{cuE} \\ \left[f_{cuE}(\varepsilon_{cuF} - \varepsilon_c) + f_{cuF}(\varepsilon_c - \varepsilon_{cuE})\right]/(\varepsilon_{cuF} - \varepsilon_{cuE}), \varepsilon_c > \varepsilon_{cuE} \end{cases} \quad (4)$$

where:

$$\mu = \frac{\varepsilon_c - \varepsilon_{cuD}}{\varepsilon_{cuE} - \varepsilon_{cuD}} \quad (5)$$

$$\beta = \frac{f_{cm}}{f_{cuD}} \quad (6)$$

$$\alpha = \frac{f_{cm}}{f_{cuE}} = 15 \quad (7)$$

$\alpha_{tD} = 0.50$ and $\alpha_{tE} = 0.60$ are parameters of the sinusoidal function shape,
$f_{cuE} = f_{cm}/\alpha$ and $f_{cuF} = 0.40$ MPa are compressive stresses at the points E and F, presented in Fig. 8a,
ε_{cuD}, ε_{cuE} =0.05 and ε_{cuF} = 0.20 are compressive strains at points D, E and F, respectively, presented in Fig. 8a.

Damage evolution for compression was defined through damage variable D_c, presented in Eq. (8) and illustrated in Fig. 8b:

$$D_c = 1 - \frac{f_{cm}}{\sigma_c} \quad (8)$$

The stress-strain relation for concrete subjected to uniaxial tension was derived from the following relation between the stress and crack opening w [27,28]:

$$\sigma_t(w) = f_{ctm}\left[g(w) - \left(\frac{w}{w_c}\right)g(w_c)\right] \quad (9)$$

where:
f_{ctm} is the mean value of the concrete tensile strength,

$$g(w) = \left[1 + \left(\frac{3w}{w_c}\right)^3\right]e^{-\frac{6.93w}{w_c}} \quad (10)$$

w_c is the critical value of the crack opening at which tensile stress cannot be transferred;

$$w_c = 5.14\frac{G_F}{f_{ctm}} \quad (11)$$

G_F is the fracture energy, which was adopted as the function of the concrete compressive strength and nominal aggregate size according to Model Code 1990 [29].

The relation between the crack opening and strain is dependent on the finite element characteristic length, l_{eq}, according to Eq. (11):

$$\varepsilon_t = \varepsilon_{t1} + w\cdot l_{eq} \quad (12)$$

where ε_{t1} is a tensile strain at the peak stress f_{ctm}.

As the size of finite elements inside the concrete slab varies in the range from 3 mm to 10 mm, the characteristic element length had to be obtained by model calibration. The best match between model and specimen response was accomplished with l_{eq} = 5 mm. The adopted stress-cracking strain relation is illustrated in Fig. 8c.

Similarly to compression, damage evolution for tension was defined through variable D_t [21,28]:

$$D_t = 1 - \frac{f_{ctm}}{\sigma_t} \quad (13)$$

3.2. Validation of finite element models

Developed finite element models were validated by comparing their behaviour to the response of experimental specimens. Load-vertical displacement curves for models R1 and R2, obtained through numerical simulations, are compared with experimental curves of corresponding specimens in Fig. 9. Developed models successfully replicate the double shear test, clearly distinguishing the difference in the construction joint response for two analysed orientations. Model R1 features brittle failure with a sudden drop in force after reaching the ultimate load, which was also present in all of the three tested specimens of series R1. On the opposite, the failure of model R2 is more ductile, but the ultimate load and vertical displacement at that load are smaller than for model R1, which is in agreement with the experimental findings. Values on the maximum load for test series R1 and R2 obtained through numerical simulations and experimental testing are compared in Table 4. The maximum relative difference between the numerical and mean experimental ultimate load is 4%, confirming the satisfying accuracy of the developed numerical models.

Table 4
Comparison between experimental and numerical ultimate loads

Series	Ultimate load		Ratio
	EXP	FEA	FEA/EXP
	$P_{ult,exp}$ [kN]	$P_{ult,fea}$ [kN]	$P_{ult,fea}/P_{ult,exp}$
R1	177.95	170.25	0.96
R2	136.15	138.04	1.01

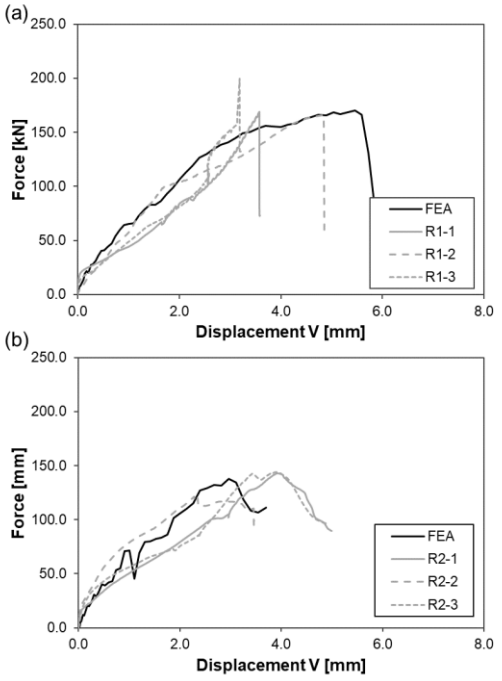

Fig. 9 Comparison between experimental and numerical force-displacement curves: (a) model R1, (b) model R2

3.3. Results of numerical analysis

Validated numerical models enabled further evaluation of the construction joint behaviour and investigation of the effect of the joint orientation on its shear performance. Comparison between force-displacement curves of models R1 and R2 presented in Fig. 10 illustrates the difference in joint response depending on whether the load is applied to the slab with the angle profile installed on its edge or to the slab with the steel plate on the edge. Up to the load of approximately 130 kN, the force-displacement relation for models R1 and R2 is almost identical, indicating that the joint orientation has no impact on the initial stiffness of the construction joint. Stiffness per steel dowel of approximately 13.0 kN/mm is almost identical for the two models. After reaching 138 kN, the load in model R2 drops, whereas the load in model R1 continues to increase until 170 kN. The construction joint with an installed steel plate in the middle (loaded) slab features postponed failure and non-negligibly increased ultimate resistance in comparison to the joint with an angle profile positioned in the middle slab, confirming the experimental findings.

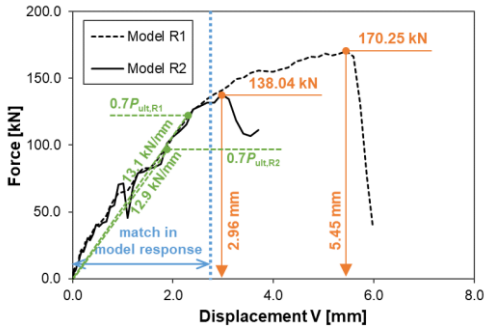

Fig. 10 Comparison between force-displacement curves for models R1 and R2

Deformed shapes of steel dowels in numerical models presenting two types of experimentally tested specimens, shown in Fig. 11, indicate larger dowel deformation in model R1 than in model R2 at the corresponding ultimate load of each model. This is in agreement with structural join vertical displacement at failure presented in Fig. 10, which is also larger for model R1. Stress distribution in steel dowels indicates the development of two plastic hinges along the dowel length. The position of plastic hinges slightly differs in the case of the two analysed joint orientations but in both cases, plastic hinges are significantly distant from the dowel ends. Accordingly, the possible reduction of dowel length should be considered, as later analysed through parametric analysis.

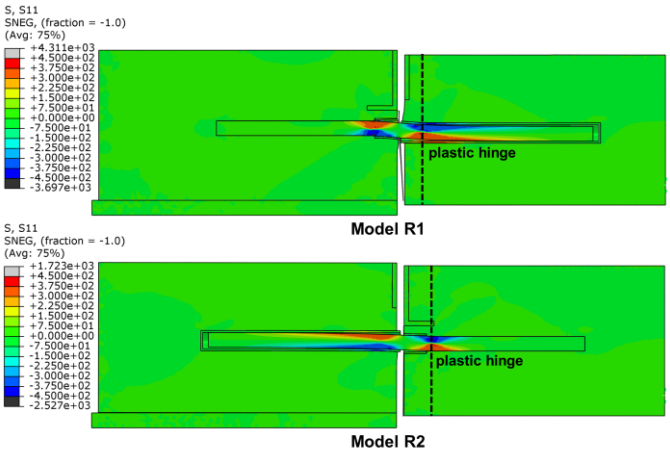

Fig. 11 Normal stress in steel dowels at the ultimate load

The levels of concrete tension and compression damage in models R1 and R2 at the point when the corresponding ultimate load is reached are compared in Fig. 12. In model R1, the concrete above the steel dowel is significantly damaged due to high compressive stresses on the contact between the dowel and surrounding concrete at the construction joint. As a result, concrete bearing causes failure of the middle slab of model R1. Unlike model R1, diagonal cracks in the concrete slab of model R2 propagate all along the construction joint from the horizontal angle leg towards the top surface of the middle slab. Their cause is associated with the presence of steel angles. The horizontal leg of the angle profile, continuous along the construction joint, disrupts the continuity of the concrete slab. It is positioned close to the steel dowel, reducing the zone of the concrete above the dowel subjected to bearing pressure and having a negative influence on the construction joint shear resistance, inducing premature failure of model R2.

To prove that the difference in shear behaviour of models R1 and R2 is solely influenced by the presence of an angle profile on the slab edge which is subjected to shear load, an additional numerical model was developed. The model R2 was modified by cutting the horizontal leg of the angle and comparing the response of such joint to the models R1 and R2. The results presented in Fig. 13 show the equivalent force-displacement responses of model R1 and modified model R2. Diagonal cracks observed in model R2 are not present in the modified model. Analogues to model R1, the governing failure mode of the modified model was concrete bearing.

It is concluded that the absence of an angle profile enhances the construction joint resistance and therefore its elimination would be favourable from the load-bearing perspective. However, the angle profile has an essential role during the construction joint execution, providing lateral stiffness and preventing formwork deformation before and during the installation process. Therefore, the consideration of the potential removal of the angle profile should be carefully approached.

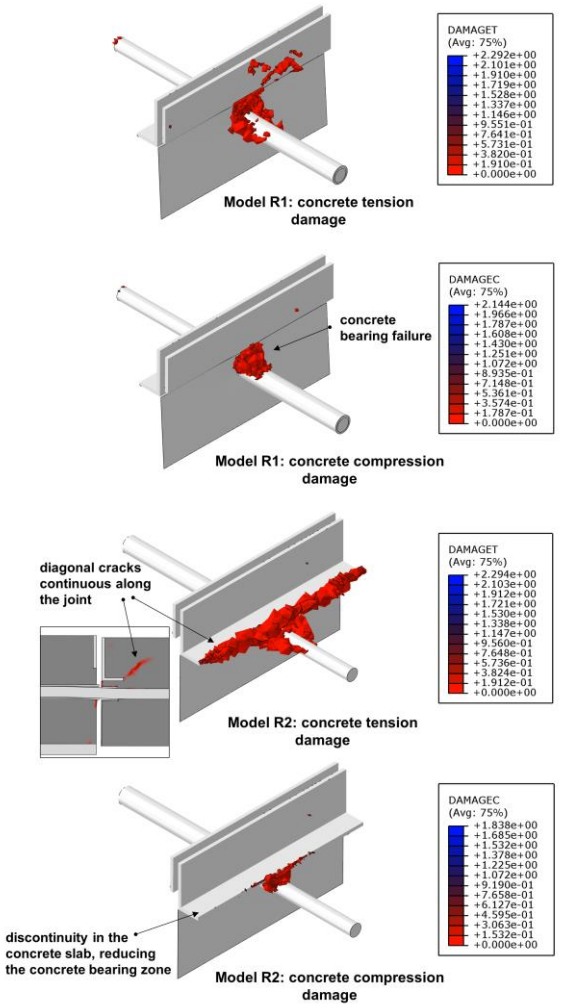

Fig. 12 Concrete damage at the ultimate load

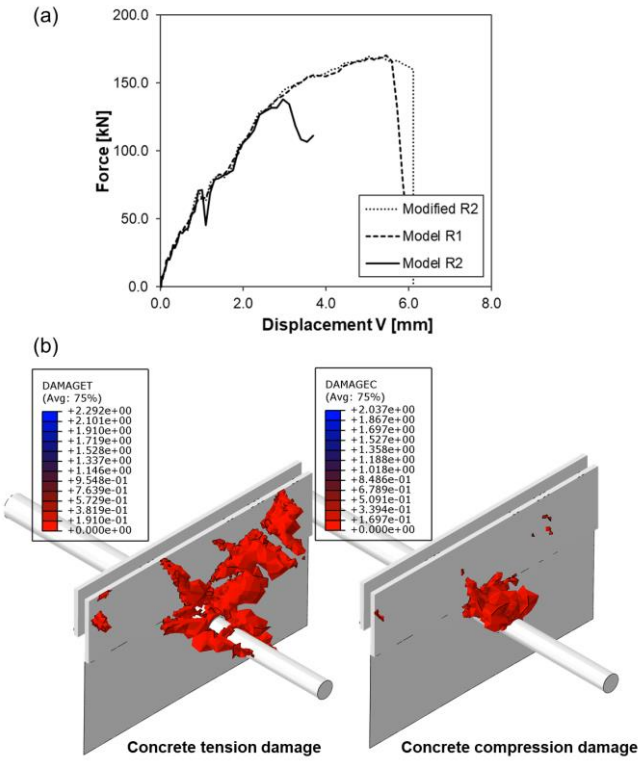

Fig. 13 Response of modified R2 model without horizontal angle leg:
(a) Force-displacement curves, (b) Concrete damage at the ultimate load

4. Parametric analysis

Validated numerical models were used for studying the effects of key material and geometric parameters on the construction joint response, including the joint opening, concrete strength, slab depth, steel dowel diameter and length. The parametric analysis was carried out for the joint orientation corresponding to model R2 since this orientation was shown to be relevant for determining joint resistance to derive safe-sided results. The primary model had the following geometrical and material properties, corresponding to the experimentally tested specimens: construction joint opening of 10 mm, concrete class C40/50, steel dowel diameter of 22 mm and length of 500 mm, and concrete slab depth of 200 mm. Through parametric analysis, each of these parameters was varied while the other parameters remained constant as in the primary model.

4.1. Effect of the construction joint opening

The experimental campaign was conducted with adjoining slabs spaced at a distance of 10 mm, replicating the construction joint opening of 10 mm caused by concrete slab shrinkage. Two additional numerical models were developed with opening sizes of 5 mm and 15 mm to observe the effect of the construction joint opening on its shear response.

Results presented in Fig. 14 show that the distribution of stress in steel dowels does not considerably change with the variation of the joint opening, but the increased deformation of steel dowels for the wider opening is evident. With the increase of opening, the joint is subjected to larger deformations and the joint stiffness is decreased. The displacement at the ultimate load rises, whereas the joint resistance decreases. Each 5 mm increase in joint opening reduces the ultimate load by around 5% and stiffness by 12–16%.

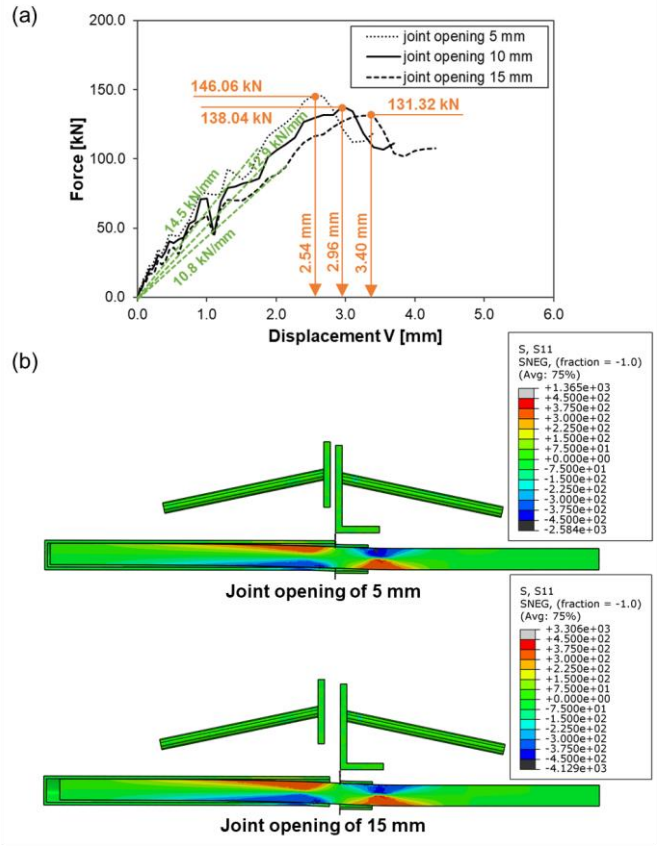

Fig. 14 Effect of the joint opening: (a) Force-displacement curves, (b) Stress in steel dowels at the failure

4.2. Effect of the concrete strength

As the governing failure mode of the analysed construction joint is the failure of concrete, the concrete strength is expected to have a major influence on the construction joint resistance. A set of numerical models with concrete classes in the range from C20/25 to C50/60 was made.

The increase in concrete strength does not significantly affect the joint stiffness according to Fig. 15a, but the increase in the resistance is considerable. For models with higher concrete strengths, the failure is postponed and ultimate loads are larger, followed by a certain increase in relative vertical displacement between the adjoining slabs. The difference in resistance between models with concrete C20/25 and C50/60 is over 30%. Ultimate loads of the analysed models presented in Fig. 15b in the function of the square root of the mean concrete strength f_{cm}, demonstrate that the resistance of the construction joint is a linear function of the $f_{cm}^{0.5}$.

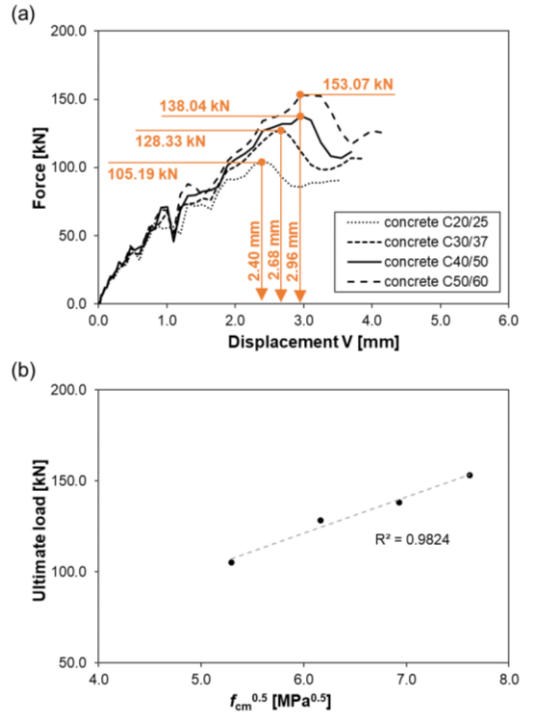

Fig. 15 Effect of the concrete strength: (a) Force-displacement curves, (b) Relation between the ultimate load and square root of the mean concrete strength

4.3. Effect of the steel dowel diameter

As the investigated construction joint with round dowels may be fabricated with varied steel dowel sizes, numerical models with dowels of diameters of 20 mm, 22 mm and 24 mm were developed and their behaviour was compared.

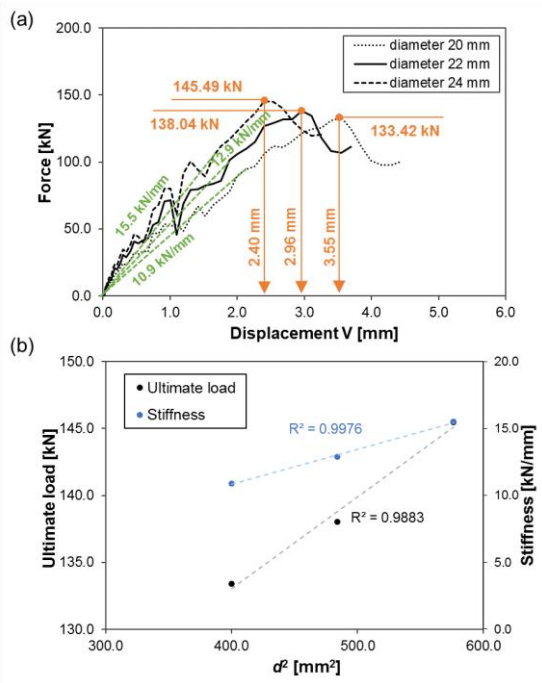

Fig. 16 Effect of the steel dowel diameter: (a) Force-displacement curves, (b) Relation between the ultimate load/stiffness and square of the dowel diameter

According to Fig. 16a, the dowel diameter affects the joint resistance, i.e.

when the diameter is increased from 20 mm to 22 mm, the rise in resistance is 3.5%, whereas, for the increase from 22 mm to 24 mm, the resistance is raised by 5.4%. Although the diameter of the steel dowel appears to have a lower effect on joint resistance than the concrete class, dowel size non-negligibly affects construction joint stiffness which varies in the range of 10.9–15.5 kN/mm for the analysed models. Fig. 16b illustrates the linear dependency between the square of the dowel diameter and the joint resistance, as well as the joint stiffness.

4.4. Effect of the steel dowel length

ACI 302.1R-04 [8] specifies dowel length depending on the floor slab depth: 400 mm for round dowels in slabs of a depth of 175–200 mm, and 450 mm for round dowels in slabs of a depth of 225–275 mm. According to this recommendation, the dowels of the analysed construction joint may be shortened. For calculating the construction joint resistance to shear according to Technical Report 34 [9], the loaded length of a steel round dowel should not be taken as greater than 8*d*, where *d* is the dowel diameter. In other words, the total effective length of a dowel could be approximated by 16*d*, accounting for both sides of the construction joint. In the particular case of the investigated construction joint, the effective steel dowel length would be around 350 mm according to this recommendation. Three additional numerical models were created with steel dowel lengths of 300 mm, 200 mm and 150 mm, to study the influence of dowel length on the joint response, and the possibility of reducing this length to optimise the construction joint.

Numerical results show little difference in the force-displacement response of construction joints with steel dowels of a length of 300 mm and 500 mm, leading to the conclusion that a reduction of the dowel length by 40% would not affect the structural performance of the construction joint. According to Fig. 17, the model with a dowel length of 200 mm also has comparable shear resistance, although force-displacement curves do not completely overlap in the pre-ultimate domain with the ones presented for longer dowels. However, when the dowel length is reduced to 150 mm, a reduction in joint resistance exceeds 20%, followed by a decrease in joint stiffness. Stress distribution in the construction joint presented in Fig. 18 shows that in the 150 mm long dowel, the plastic hinge is only developed in the right half of the dowel. This length of steel dowel is insufficient to transfer shear force between adjoining slabs in comparison to longer dowels. According to the presented results, the dowel length may be kept at 14*d* (14 · 22 mm = 308 mm ≈ 300 mm) while retaining the same construction joint response in terms of deformation and load capacity as when longer dowels are applied.

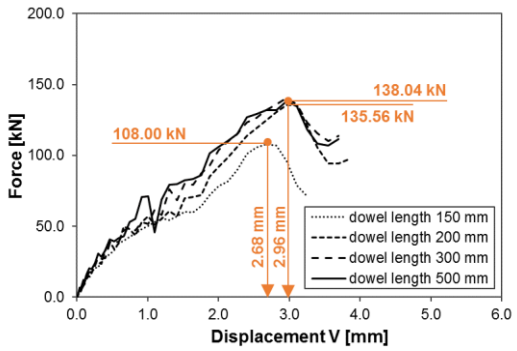

Fig. 17 Effect of the steel dowel length: Force-displacement curves

4.5. Effect of the concrete slab depth

The effect of concrete slab depth was investigated through the set of numerical models covering floor slabs with depths in the range of 180 mm to 240 mm. Steel dowels were positioned in the slab mid-depth in each of the developed models. The size of the steel plate and angle profile remained unchanged, while their position was linked to the upper surface of the concrete slab, meaning the distance between the angle profile and steel dowel was increased with the increase of the slab depth.

The increase in slab depth significantly increased the construction joint resistance, although the stiffness remained unchanged, as presented in Fig. 19a. The decrease in slab depth to 180 mm from the original 200 mm, caused a drop in ultimate load of 4%, while the increase to 220 mm led to the rise of almost 12%. All three of these models featured similar shape force-displacement curves without a sudden decline of force in the post-ultimate domain. The additional increase of the slab depth to 240 mm, improved the shear resistance by 30% in comparison to the model with a slab depth of 200 mm. However, a model with a 240 mm deep slab showed a different force-displacement response with brittle failure and rapid force drop after reaching its maximum, similar to the one observed in model R1 with the opposite joint orientation.

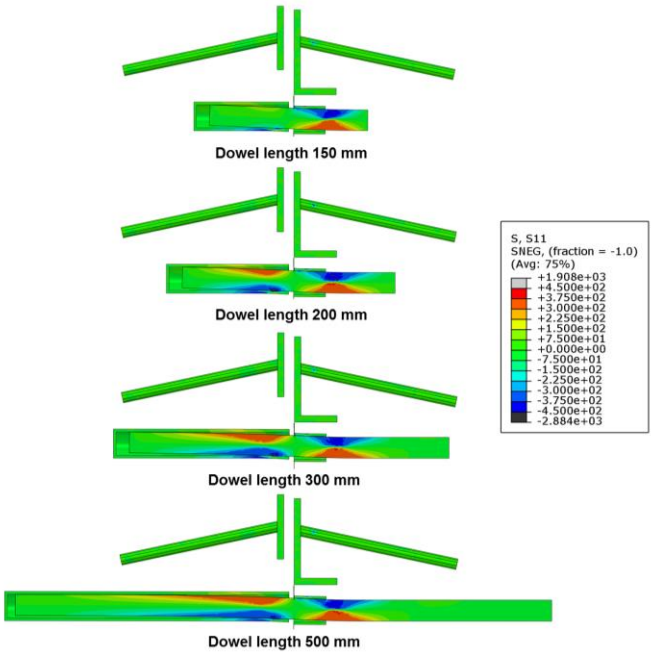

Fig. 18 Effect of the steel dowel length: Stress in steel dowels at the failure

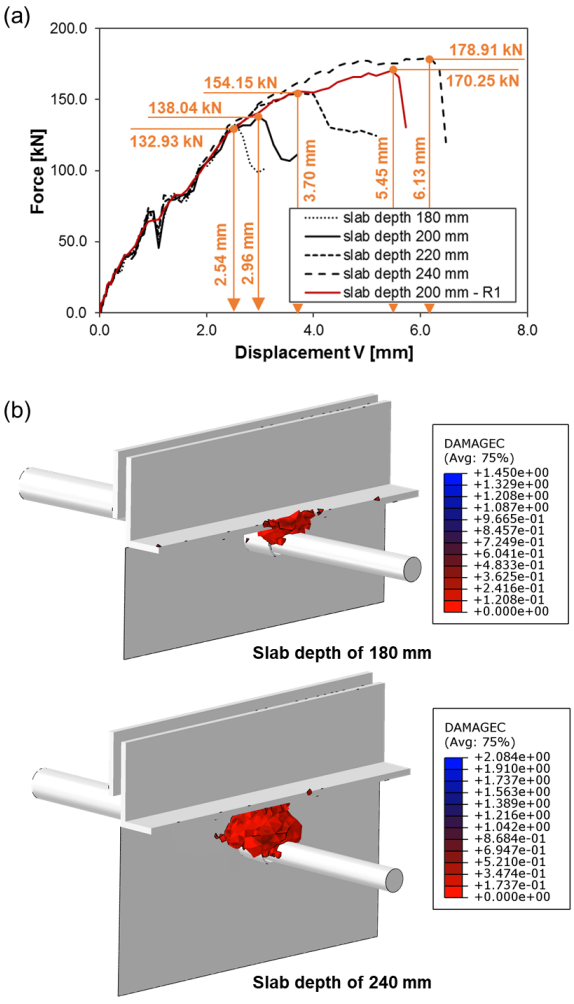

Fig. 19 Effect of the concrete slab depth: (a) Force-displacement curves, (b) Concrete compression damage at the failure

Concrete damage in slabs of a depth of 180 mm and 240 mm, presented in Fig. 19b, illustrates the differences in the response of construction joints in those two cases. When the slab depth is larger, the distance between the angle profile and steel dowel is also greater, causing the distribution of bearing stresses in concrete similar to the one in the construction joint with a 60 x 6 mm steel plate in the slab subjected to failure (model R1). On the opposite, with a decrease in the slab depth and spacing between the angle profile and steel dowel, the construction join resistance is reduced due to the discontinuity in the bearing concrete influenced by the horizontal angle leg. Therefore, the slab thickness is an important factor affecting the shear behaviour of the investigated construction joint including the angle profile that is continuous along the slab edge.

5. Conclusions

The integral solution of the free-movement construction joint developed for application in concrete industrial ground floors was experimentally and numerically investigated. The construction joint shear behaviour was studied considering two joint orientations through the experimental campaign, and covering five additional influential parameters through finite element simulations. According to the obtained results, the following conclusions could be drawn:

(1) Construction joint orientation does not affect stiffness, but it influences joint resistance and post-ultimate behaviour. When failure occurs in the concrete slab with an angle profile installed on the slab edge, construction joint resistance is decreased by more than 20% in comparison to the opposite case when the slab with a steel plate is subjected to failure. Joint failure in the concrete slab with steel plate is highly brittle, unlike the joint failure in the slab with angle profile, which is more ductile.

(2) Differences in construction joint response for opposite joint orientations are attributed to different steel components on the slab edges in those two cases: steel plate and angle profile. The horizontal leg of the angle profile cuts through the slab, causing discontinuity in the concrete and resulting in the development of diagonal cracks along the construction joint. If steel dowels are positioned directly below the angle profile, the concrete zone above the dowel is insufficient to bear compression stresses, inducing the earlier failure of the joint.

(3) Construction joint opening caused by concrete slab dry shrinkage affects the bending deformation of steel dowels, as well as the construction joint stiffness and resistance. For the analysed construction joint, the 5 mm increase in the joint opening results in approximately 5% lower joint resistance and 12–16% lower joint stiffness.

(4) The increase in concrete strength improves the construction joint resistance. This increase is proportional to the square root of the concrete compressive strength. Moreover, the diameter of the steel dowel affects the construction joint stiffness and resistance. The increases in resistance and stiffness are both proportional to the square of the dowel diameter.

(5) The construction join response remains the same when the dowel length is varied between 300 mm and 500 mm, meaning that for the analysed dowel, the reduction of dowel length to 14*d* does not affect the joint deformation and load capacity. However, a further decrease in length below 200 mm induces a considerable drop in the stiffness and resistance.

(6) Concrete slab depth significantly affects the construction joint resistance. As the slab depth increases, the vertical distance between the steel dowel and the angle profile gets larger, reducing the negative impact of the angle profile and influencing the higher resistance of the joint. As a result, increasing the slab depth from 200 mm to 240 mm can increase joint resistance by 30%.

Funding

This investigation was supported by the Innovation Fund of the Republic of Serbia, through the Innovation voucher programme (Voucher No. 1397, 2023).

Acknowledgements

The authors are grateful to the company Rinol d.o.o, Belgrade, for their support.

References

[1] Al-Humeidawi BH, Mandal P. Experimental investigation on the combined effect of dowel misalignment and cyclic wheel loading on dowel bar performance in JPCP. Engineering Structures 2018;174:256–66. https://doi.org/10.1016/j.engstruct.2018.07.052.
[2] Al-Humeidawi BH, Mandal P. Evaluation of performance and design of GFRP dowels in jointed plain concrete pavement – part 1: experimental investigation. International Journal of Pavement Engineering 2014;15:449–59. https://doi.org/10.1080/10298436.2013.824081.
[3] Fasil M, Rahman MK, Al-Zahrani MM, Nanni A, Najamuddin SK. Load transfer of small-diameter GFRP and stainless steel doweled-joints in slabs-on-ground. Engineering Structures 2024;302:117241. https://doi.org/10.1016/j.engstruct.2023.117241.
[4] Al-Humeidawi BH, Mandal P. Numerical evaluation of the combined effect of dowel misalignment and wheel load on dowel bars performance in JPCP. Engineering Structures 2022;252:113655. https://doi.org/10.1016/j.engstruct.2021.113655.
[5] Zuzulova A, Grosek J, Janku M. Experimental Laboratory Testing on Behavior of Dowels in Concrete Pavements. Materials 2020;13:2343. https://doi.org/10.3390/ma13102343.
[6] Shalaby A. Using fiber-reinforced polymer load transfer devices in jointed concrete pavements, Orlando, Florida, USA: 2001.
[7] Vijay PV, Li H, GangaRao VH. Laboratory testing, field construction, and decade long performance evaluation of jointed plain concrete pavement with FRP dowels. International Journal of Pavement Engineering 2020;21:713–24. https://doi.org/10.1080/10298436.2018.1508841.
[8] ACI Committee 302. ACI 302.1R-04 Guide for Concrete Floor and Slab Construction. Farmington Hills: American Concrete Institute; 2004.
[9] Concrete Society Project Steering Committee and Design sub-group. Technical Report 34 Concrete industrial ground floors - a guide to their design and construction. Camberley: The Concrete Society; 2013.
[10] Li YL, Li LK, Tan YQ, Xue ZJ. Performance Properties of GFRP Dowels in Concrete Pavement Joints. Applied Mechanics and Materials 2012;178–181:1147–51. https://doi.org/10.4028/www.scientific.net/AMM.178-181.1147.
[11] Al-Humeidawi BH, Mandal P. Evaluation of performance and design of GFRP dowels in jointed plain concrete pavement – part 2: numerical simulation and design considerations. International Journal of Pavement Engineering 2014;15:752–65. https://doi.org/10.1080/10298436.2014.893314.
[12] Mackiewicz P. Analysis of stresses in concrete pavement under a dowel according to its diameter and load transfer efficiency. Can J Civ Eng 2015;42:845–53. https://doi.org/10.1139/cjce-2014-0110.
[13] Sadeghi V, Hesami S. Investigation of load transfer efficiency in jointed plain concrete pavements (JPCP) using FEM. International Journal of Pavement Research and Technology 2018;11:245–52. https://doi.org/10.1016/j.ijprt.2017.10.001.
[14] Grosek J, Zuzulova A, Brezina I. Effectiveness of Dowels in Concrete Pavement. Materials 2019;12:1669. https://doi.org/10.3390/ma12101669.
[15] EN1994-1-1. Eurocode 4: Design of composite steel and concrete structures. Part 1-1: General rules and rules for buildings. Brussels: CEN; 2004.
[16] ISO6892-1:2009. Metallic materials - Tensile testing - Part 1: Method of test at room temperature. Brussels: CEN; 2009.
[17] EN1990:2010. Eurocode - Basis of structural design. Brussels: CEN; 2010.
[18] Abaqus/CAE. User's Guide. Providence: DS SIMULIA Corp.; 2009.
[19] EN1992-1-1. Eurocode 2: Design of Concrete Structures. Part 1-1: General rules and rules for buildings. Brussels: CEN; 2004.
[20] Lubliner J, Oliver J, Oller S, Oñate E. A plastic-damage model for concrete. International Journal of Solids and Structures 1989;25:299–326. https://doi.org/10.1016/0020-7683(89)90050-4.
[21] Pavlović M, Marković Z, Veljković M, Buđevac D. Bolted shear connectors vs. headed studs behaviour in push-out tests. Journal of Constructional Steel Research 2013;88:134–49. https://doi.org/10.1016/j.jcsr.2013.05.003.
[22] Spremic M, Pavlovic M, Markovic Z, Veljkovic M, Budjevac D. FE validation of the equivalent diameter calculation model for grouped headed studs. Steel and Composite Structures 2018;26:375–86. https://doi.org/10.12989/scs.2018.26.3.375.
[23] Gluhović N. Behaviour of shear connections realised by connectors fastened with cartridge fired pins. University of Belgrade, 2019.
[24] Žuvelek V, Ćurković I, Lukačević I, Rajić A. Finite Element Analyses of Demountable Shear Connection in Cold-Formed Steel-Concrete Composite Beam Based on Experimental Data. Ce/Papers 2023;6:213–9. https://doi.org/10.1002/cepa.2629.
[25] Jakovljević I, Spremić M, Marković Z. Shear behaviour of demountable connections with bolts and headed studs. Advanced Steel Construction 2023;19:341–52. https://doi.org/10.18057/IJASC.2023.19.4.3.
[26] Jakovljević I, Spremić M, Marković Z. Effect of rib-to-beam angle on the shear resistance of headed studs in composite slab. Engineering Structures 2024;303:117574. https://doi.org/10.1016/j.engstruct.2024.117574.
[27] Birtel V, Mark P. Parameterised Finite Element Modelling of RC Beam Shear Failure. ABAQUS Users' Conference, 2006, p. 95–108.
[28] Vigneri V, Odenbreit C, Lam D. Different load bearing mechanisms in headed stud shear connectors for composite beams with profiled steel sheeting. Steel Construction 2019;12:184–90. https://doi.org/10.1002/stco.201900019.
[29] CEB-FIP. Model Code 1990. London: Thomas Telford Services Ltd; 1993.